ACS APPLIED MATERIALS & INTERFACES

RESEARCH ARTICLE

www.acsami.org

Modifying Fe_3O_4-Functionalized Nanoparticles with *N*-Halamine and Their Magnetic/Antibacterial Properties

Alideertu Dong,[†] Shi Lan,[‡] Jinfeng Huang,[§] Tao Wang,[†] Tianyi Zhao,[†] Linghan Xiao,[†] Weiwei Wang,[†] Xin Zheng,[†] Fengqi Liu,[†] Ge Gao,[*,†] and Yuxin Chen[*,§]

[†]College of Chemistry, Jilin University and MacDiarmid Laboratory, Changchun 130021, People's Republic of China

[‡]College of Chemistry and Chemical Engineering, Inner Mongolia University for the Nationalities, Tongliao 028000, People's Republic of China

[§]Key Laboratory for Molecular Enzymology and Engineering of the Ministry of Education, Jilin University, Changchun 130012, People's Republic of China

ABSTRACT: Magnetic/antibacterial bifunctional nanoparticles were fabricated through the immobilization of antibacterial *N*-halamine on silica-coated Fe_3O_4-decorated poly(styrene-*co*-acrylate acid) (PSA) nanoparticles. The samples were characterized by scanning electron microscopy (SEM), transmission electron microscopy (TEM), X-ray photoelectron spectra (XPS), X-ray diffraction (XRD), energy-dispersive X-ray spectrometry (EDX), Fourier transform infrared (FTIR), and thermogravimetric analysis (TGA). The *N*-halamine was developed from the precursor 5,5-dimethylhydantoin (DMH) by chlorination treatment, and experimental results showed that the loading amount of DMH on the silica-coated Fe_3O_4-decorated poly(styrene-*co*-acrylate acid) nanoparticles was adjustable. The as-synthesized nanoparticles exhibited superparamagnetic behavior and had a saturation magnetization of 18.93 emu g^{-1}. Antibacterial tests showed that the resultant nanoparticles displayed enhanced antibacterial activity against both Gram-positive and Gram-negative bacteria compared with their bulk counterparts.

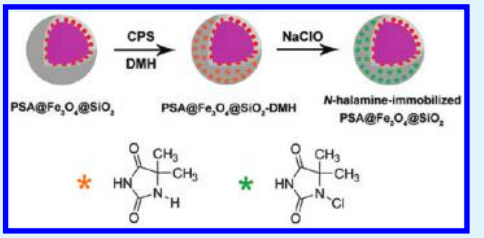

KEYWORDS: *N*-halamine, SiO_2, Fe_3O_4, poly(styrene-*co*-acrylate acid), nanoparticles, bifunctional

INTRODUCTION

Recently, microbial threats on human health and safety have become a serious public concern. In response to the wide spreading of infectious diseases, antibacterial materials that can effectively inhibit the growth of microorganisms have attracted significant research interests.[1] To date, free halogen,[2−4] ozone,[5,6] chlorine oxide,[7,8] metal ions,[9] quaternary ammonium salts,[10,11] quaternary phosphonium salts,[12] molecularly engineered peptides,[13] guanidine,[14,15] *N*-chlorinated sulfonamides,[16] *N*-halamines,[17,18] etc., have been used in the development of antibacterial materials. The antibacterial performances of these materials differ significantly, offering considerably broad selective options for a wide range of application fields.[19] It was established in the mid 1970s that *N*-halamines are excellent antibacterial compounds for several reasons including antibacterial efficacies, stabilities in aqueous solution and in dry storage, lack of corrosion of surfaces, low toxicities, and relatively low expense.[20,21] Extensive work on *N*-halamine compounds for disinfection in aqueous solution was reported during the 1980s, illustrating their potential for use in a broad variety of applications.[22−24] The most important practical application for *N*-halamine compounds has been directed toward inactivation of pathogens.[25] Worley and co-workers have focused on the development of novel *N*-halamines for use in potable water disinfection and textiles for several decades.[22−25] In more recent times, *N*-halamine materials have been developed and investigated extensively in several laboratories.[21,26−28] In other words, stable *N*-halamines are effective oxidizing agents that can oxidize the molecules on cell surfaces which are vital for cell survival.[28] Therefore, *N*-halamine chemistry has proved to be important in the development of effective antibacterial compounds.

Great efforts have been devoted to synthesizing multicomponent hybrid nanoparticles, which were explored as a means to achieve increased complexity and functionality in nanoparticles.[29−31] These nanoparticles are composed of discrete domains of different components, and thus can exhibit the properties of different components in the same structure.[32] Such hybrid nanoparticles open up new possibilities for investigating the synergism between different nanoscale components, and have a broad range of applications not available in homogeneous nanoparticles.[33] Among multifarious hybrid nanoparticles, multifunctional nanoparticles with magnetic component have received much attention from researchers due to their various biological and medicinal applications, such as magnetic targeting of drugs, genes, and radiopharmaceuticals; magnetic resonance imaging; diagnostics; immunoassays; RNA and DNA purification; gene cloning; and cell separation and purification.[34−38] Magnetic component provided hybrid nanoparticles mobility in the presence of a magnetic field.[39] Fe_3O_4 nanoparticles are most commonly selected as superparamagnetic

Received: July 1, 2011
Accepted: October 18, 2011
Published: October 18, 2011

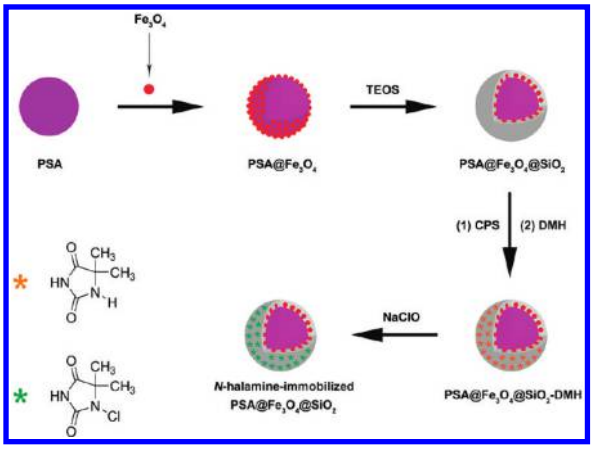

Figure 1. Schematic illustration of the preparation procedure of the *N*-halamine-immobilized $PSA@Fe_3O_4@SiO_2$ nanoparticles.

component in the fabrication of the multifunctional hybrid nanoparticles because of their unique magnetic properties and ease of preparation.[40] In particular, Fe_3O_4 nanoparticles prepared by the well-known Massart's method based on the classical coprecipitation procedure is most widely used superparamagnetic nanoparticles.[41]

Hybrid nanoparticles with a controllable shape and size are of great scientific and technological importance because of their unique chemical and physical properties.[42] A colloidal template method is an effective and general approach for the preparation of structure governable nanoparticles, especially for studies in which a narrow size distribution is required.[43] The apparent advantage of the colloidal template method is that the shape and size of formed nanostructures are directly determined by the template.[44] Monodisperse poly(styrene-acrylic acid) (PSA) nanoparticles are commonly chosen as colloidal templates because they are prepared simply by the surfactant-free emulsion polymerization, and easily controllable in a wide range of sizes.[45−47] For example, Li et al. reported the study of using monodisperse PSA nanoparticles to produce surface-enhanced Raman spectroscopy (SERS) labels with the aim to improve the synthetic control over the micro/nano structures of the SERS substrates for high performance molecular imaging and molecular barcode applications.[45] Xuan et al. designed well-defined magnetic separable, hollow spherical Fe_3O_4/TiO_2 hybrid photocatalysts by the aid of PSA template.[46] Lu et al. synthesized monodisperse magnetizable silica composite particles from the heteroaggregates of PSA nanoparticles and Fe_3O_4 nanoparticles.[48]

Herein, novel bifunctional hybrid nanoparticles were prepared through anchoring antibacterial *N*-halamine on silica-coated magnetic nanoparticles by the aid of PSA template. The procedure employed to obtain *N*-halamine-immobilized $PSA@Fe_3O_4@SiO_2$ nanoparticles is illustrated in Figure 1. First, monodisperse PSA nanoparticles were synthesized by surfactant-free emulsion polymerization method, and Fe_3O_4 nanoparticles were deposited on PSA nanoparticles to make them magnetically functionalized. To achieve highly stable magnetic nanoparticles, $PSA@Fe_3O_4$ nanoparticles were encapsulated by thin silica shell. The surface of the silica-coated $PSA@Fe_3O_4$ nanoparticles were subsequently modified with a silane coupling agent (3-chloropropyl triethoxysilane, CPS), and chlorine groups on the surface of $PSA@Fe_3O_4@SiO_2$ nanoparticles are so active that they can easily attach to 5,5-dimethylhydantoin (DMH, the precursor of *N*-halamine). Finally, the hydantoin groups of DMH transformed into *N*-halamine structures by chlorination treatment to produce *N*-halamine-immobilized silica-coated magnetic PSA nanoparticles. Successful preparation was evidenced by different techniques like SEM, TEM, XPS, EDX, XRD, FTIR, and TGA. The resultant hybrid nanoparticles exhibited satisfying magnetic property and powerful antibacterial activity against both Gram-positive and Gram-negative bacteria. The synergism between these two functions can prevent the magnetic materials from microbial threats, and make the antibacterial agents magnetically governable. It is a promising topic to synthesize hybrid nanoparticles consisting of the several kinds of components with fine structures and excellent antibacterial/magnetic properties.

EXPERIMENTAL SECTION

Materials. Ferric chloride ($FeCl_3$) was purchased from Tianjin Huadong Chemical Reagent Plant. Ferrous chloride ($FeCl_2 \cdot 4H_2O$), styrene (St), Acrylic acid (AA), and tetraethoxysilane (TEOS) were obtained from Tianjin Guangfu Fine Chemical Research Iinstitute. Anhydrous ethanol, methanol and ammonium hydroxide (25 wt % NH_3 in water) were purchased from Beijing Chemical Company. 3-chloropropyl trimethoxysilane (CPS), potassium persulfate (PPS) and Sodium bicarbonate ($NaHCO_3$) were available from Shanghai Chemical Reagent Plant and Tianjin Hongyan Chemical Reagent Factory, respectively. Potassium hydroxide (KOH) and sodium hypochlorite (NaClO) were provided from Sinopharm Chemical Reagent Co., Ltd. 5, 5-dimethylhydantoin (DMH) was purchased from Westingarea Co., Ltd. The other reagents were analytical grade and were used without any purification.

Preparation of Fe_3O_4 Nanoparticles. Iron oxide nanoparticles (Fe_3O_4) were prepared through an improved chemical coprecipitation method.[48] Briefly, a solution of a mixture of $FeCl_3$ (1.817 g) and $FeCl_2 \cdot 4H_2O$ (1.113 g) together with 150 mL of water was prepared with agitation under N_2 protection in a three-necked flask of 250 mL volume. Then, 15 mL of NH_3 aqueous solution (25 wt %) was added dropwise slowly to the flask. After reacting at 50 °C for 30 min under mechanical stirring and N_2 protection, the Fe_3O_4 solid precipitations were magnetically separated, washed with water for dozens of times.

Preparation of PSA Nanoparticles. PSA nanoparticles were prepared by surfactant free emulsion copolymerization of St with AA.[49] Typically, 100 mL of water, 0.12 g of $NaHCO_3$, 5 mL of St and 0.5 mL of AA were added into a three-necked flask fitted with a reflux condenser and a mechanical stirrer. PPS served as the initiator and no surfactant was used in the polymerization. The reaction was carried out under a nitrogen atmosphere at 70 °C for 12 h with mechanical stirring. The resulting product was purified by several centrifugation/dispersion cycles in water.

Preparation of $PSA@Fe_3O_4$ Nanoparticles. Stock solution with pH value of 2−4 was prepared by the addition of hydrochloric acid in water. The PSA and Fe_3O_4 nanoparticles were washed with the stock solution, and then dispersed in the stock solution by ultrasonic treatment. One mL of PSA (10 mg/mL) dispersion was added to a 5 mL dispersion of Fe_3O_4 nanoparticles (6 mg/mL) under vigorous stirring. After 6 h, the $PSA@Fe_3O_4$ were separated from the solution by magnetic decantation and washed several times with a 1:1 (V:V) mixture of water and ethanol to remove nonadsorbed Fe_3O_4 nanoparticles.

Preparation of $PSA@Fe_3O_4@SiO_2$ Nanoparticles. The Stöber method was used for depositing a silica layer on $PSA@Fe_3O_4$ nanoparticles.[50] Typically, 1 mL of the $PSA@Fe_3O_4$ (10 mg/mL), 50 mL of ethanol, and 300 μL of TEOS were added into a 250 mL three-necked flask, and the mixture was stirred vigorously at room temperature. After 24 h, a mixture of 1 mL of water and 1.7 mL of ammonium hydroxide was added into the flask and allowed to react for 12 h. The resulting

composite particles were isolated from the solution by magnetic decantation and washed several times with water.

Preparation of PSA@Fe_3O_4@SiO_2-DMH Nanoparticles. Immobilization of DMH on PSA@Fe_3O_4@SiO_2 nanoparticles was accomplished via a two-step process including CPS modification of PSA@Fe_3O_4@SiO_2 nanoparticles and DMH immobilization. First, the surfaces of PSA@Fe_3O_4@SiO_2 nanoparticles were modified with 3-chloropropyl triethoxysilane (CPS). Briefly, 0.5 g of PSA@Fe_3O_4@SiO_2 nanoparticles was mixed with 0.1 mL of CPS and 25 mL of ethanol at 40 °C for 12 h. The CPS-modified PSA@Fe_3O_4@SiO_2 colloids were separated with a magnet and washed repeatedly with ethanol and water to remove excess CPS.

In the second step, 0.1 g of DMH was dissolved in 20 mL of ethanol in the presence of 0.1 g of potassium hydroxide. This mixture was heated at 78 °C for 30 min, after 0.5 g of CPS modified PSA@Fe_3O_4@SiO_2 nanoparticles and 10 mL of methanol were added into the mixtures. The reaction was continued for 12 h at 60 °C. The products PSA@Fe_3O_4@SiO_2-DMH were collected by magnetic decantation and washed by repeating redispersion in deionized water and pure ethanol, respectively.

Preparation of *N*-Halamine-Immobilized PSA@Fe_3O_4@SiO_2 Nanoparticles. Chlorination of PSA@Fe_3O_4@SiO_2-DMH nanoparticles was carried out as followed. About 0.2 g of PSA@Fe_3O_4@SiO_2 was dispersed into 20 mL of sodium hypochlorite solution, and chlorination was carried out by vigorously stirring for 12 h at room temperature. In the end, the products *N*-halamine-immobilized PSA@Fe_3O_4@SiO_2 were separated with a magnet and washed by repeating redispersion in deionized water and pure ethanol.

Characterizations. TEM images were taken on a Hitachi H-8100 transmission electron microscope at 200 kV. SEM images were taken on a Shimadzu SSX-550 field emission scanning electron microscope at 15.0 kV. The energy-dispersive X-ray (EDX) was also performed during the scanning electron microscope measurements. The XRD patterns were obtained with a Siemens model D5000 diffractometer equipped with a copper anode producing X-rays with a wavelength of 1.5418 Å. Data were collected in continuous scan mode from 10 to 80° with a 0.02° sampling interval. X-ray photoelectron spectra (XPS) measurement was carried out on a PHI-5000CESCA system with Mg K radiation (hr =1253.6 eV). The X-ray anode was run at 250 W, and the high voltage was kept at 14.0 kV with a detection angle at 540. All the binding energies were calibrated by using the containment carbon (C 1s = 284.6 eV). FTIR spectra were recorded by using a Thermo Nicolet (Woburn, MA) Avatar 370 FTIR spectrometer. Thermogravimetric analysis (TGA) was performed suing a PerkinElmer thermogravimetric analyzer. Magnetization curves as a function of magnetic field were measured at 298 K under magnetic field up to 10 kOe.

Antibacterial Test. Control and chlorinated samples were challenged with *Staphylococcus aureus* (*S. aureus*, ATCC 25923, Gram-positive) and *Pseudomonas aeruginosa* (*P. aeruginosa*, ATCC 27853, Gram-negative) using the spread plate method. Bacteria were grown overnight at 37 °C in Luria−Bertani medium (LB, 10 g of tryptone and 5 g of yeast extract/liter). Cells were harvested by centrifugation, washed twice with phosphate-buffered saline (PBS, NaCl, 8.0 g/L; KCl, 0.20 g/L; $Na_2HPO_4 \cdot 12H_2O$, 3.49 g/L; KH_2PO_4, 0.2 g/L; pH 7.4), and diluted to concentrations of $1 \times 10^{6-7}$ colony-forming units/mL. 100 mg of each sample was dispersed in 0.45 mL sterilized distilled water, vortexed, and then sonicated for 30 min. For antibacterial test, 50 μL of bacteria suspension was added into 450 μL sample suspension (final concentration of 200 mg/mL), mixed well, and incubated on a rotary shaker with the rotation speed of 170 rpm. After a certain period of contact time, 4.5 mL of 0.03 wt % sodium thiosulfate aqueous solution, sterilized by passing through 0.22 μm membrane and exhibited no effect on the growth of bacteria, was added into the reaction suspension to neutralize the active chlorine and stop the antibacterial action of sample. The resulting mixture was mixed well, serially diluted, and then 100 μL of each dilution was dispersed onto LB agar plates. Colonies on the plates were counted after incubation at 37 °C for 24 h. Bacteria diluted by diwater in the same way of sample testing (blank solution) worked as negative control.

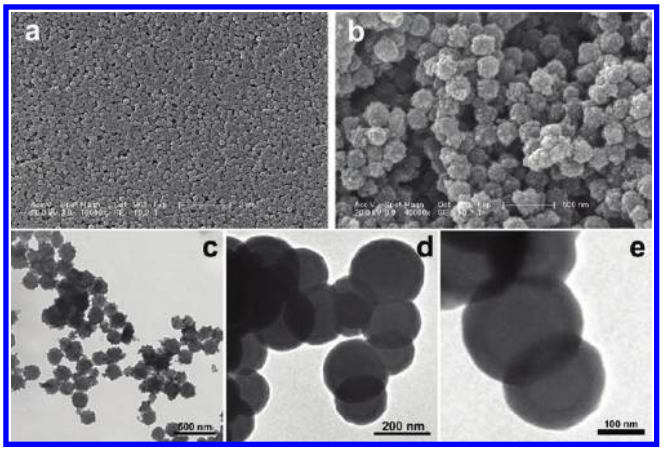

Figure 2. SEM images of (a) PSA and (b) PSA@Fe_3O_4, and (c) TEM images of PSA@Fe_3O_4, (d) PSA@Fe_3O_4@SiO_2, and (e) *N*-halamine-immobilized PSA@Fe_3O_4@SiO_2 nanoparticles.

Minimum inhibitory concentration (MIC) and minimum bactericidal concentration (MBC) were also determined to evaluate the antibacterial activity of the sample. Bacteria were grown overnight at 37 °C in Mueller Hinton Broth (MHB). Cells were harvested by centrifugation, washed twice with MHB and diluted to concentrations of 2×10^6 colony-forming units/mL Samples with serial weights were each dispersed in 150 μL MHB, vortexed, and then sonicated for 30 min. 50 μL of bacteria suspension was then added into sample suspension. After incubation in a shaking incubator overnight at 37 °C, 1.8 mL of 0.03 wt % sodium thiosulfate aqueous solution was added into the incubation suspension. The resulting mixture was serially diluted, and then 100 μL of each dilution was dispersed onto LB agar plates. Colonies on the plates were counted after incubation at 37 °C for 24 h.

RESULTS AND DISCUSSION

The morphology and sizes of the sample were observed by SEM and TEM as shown in Figure 2. Figure 2a shows representative SEM image of the pristine PSA nanoparticles, exhibiting that monodisperse and well-defined spherical particles with average particle diameter of 171 ± 10.2 nm have smooth surfaces without any coagulation. In images b and c in Figure 2, PSA@Fe_3O_4 nanoparticles possess rough surfaces, distinctively suggesting that Fe_3O_4 nanoparticles are irregularly dispersed on the PSA surfaces. The particle sizes of the iron oxide nanoparticles are in the range of 6−30 nm. On the basis of SEM and TEM analysis, a powerful evidence for the stability of PSA@Fe_3O_4 nanoparticles was presented. PSA@Fe_3O_4 nanoparticles fabricated at low pH kept their original structure under neutral condition of TEM study, indicating that interactions other than electrostatic ones exist at the interface of the PSA and Fe_3O_4 nanoparticles which are responsible for the stability of the PSA@Fe_3O_4 nanoparticles.[48] Silica-coated PSA@Fe_3O_4 nanoparticles as shown in Figure 2d exhibit spherical shape, smooth surface, and obvious core/shell structure, implying the uniform coating of silica layer. TEM observations also show that the mean diameter of the composite nanoparticles increases to about 228 nm after the silica coating, and the increase in particle size is also an evidence of the presence of silica shell. TEM image of

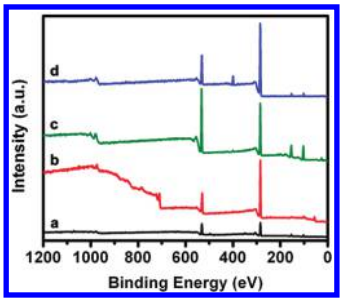

Figure 3. XPS spectra of (a) PSA, (b) PSA@Fe_3O_4, (c) PSA@Fe_3O_4@SiO_2, (d) PSA@Fe_3O_4@SiO_2-DMH nanoparticles.

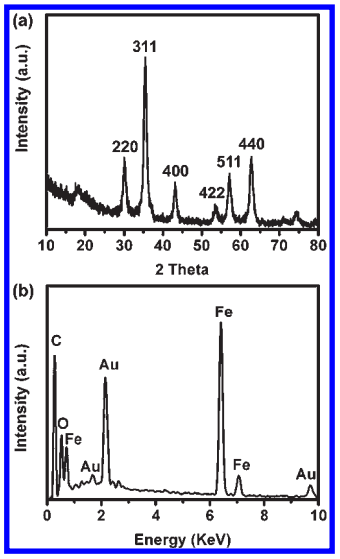

Figure 4. (a) XRD and (b) EDX spectra of PSA@Fe_3O_4 nanoparticles.

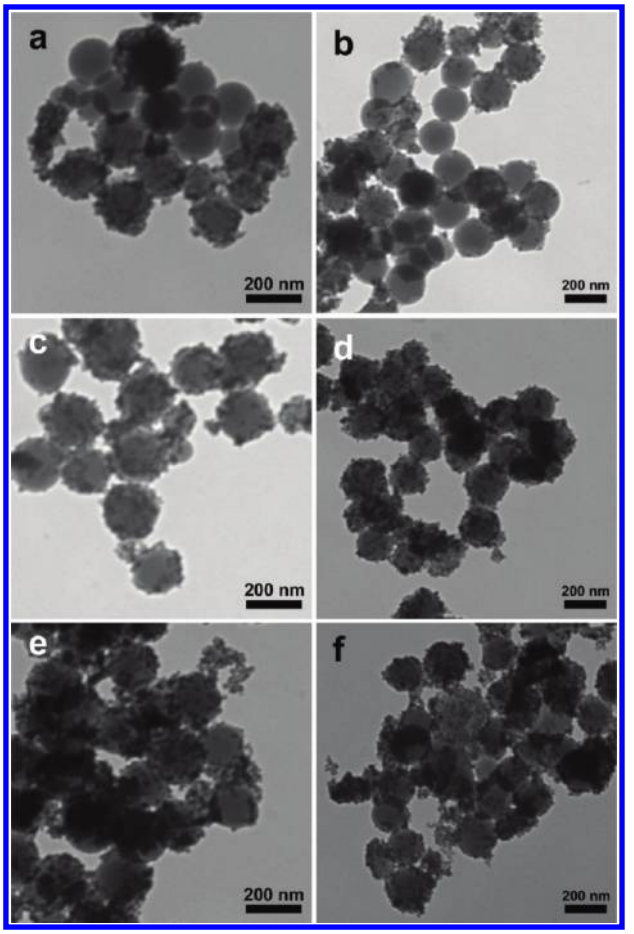

Figure 5. TEM images of PSA@Fe_3O_4 nanoparticles prepared with different Fe_3O_4/PSA mass ratio: (a, b) 1/1, (c, d) 3/1, and (e, f) 5/1.

the *N*-halamine-immobilized PSA@Fe_3O_4@SiO_2 nanoparticles is shown in Figure 2e. Composite particles maintain spherical shape and core/shell structure, and particles surfaces become somewhat coarseness, which distinctly expresses that *N*-halamine is loaded onto the surface of PSA@Fe_3O_4@SiO_2 nanoparticles.

Detailed information about the composition of the samples was provided by X-ray photoelectron spectroscopy (XPS) measurements. XPS spectra of PSA, PSA@Fe_3O_4, PSA@Fe_3O_4@SiO_2, and PSA@Fe_3O_4@SiO_2-DMH nanoparticles were shown in Figure 3. The PSA nanoparticles show the main peaks of C 1s and O 1s centered at 284 and 533 eV, respectively.[51] As for PSA@Fe_3O_4, additional new peaks of Fe $2p_{3/2}$ and Fe $2p_{1/2}$ appeared at 710 and 724 eV, indicating that Fe_3O_4 nanoparticles successfully deposited on PSA surfaces.[52] In the spectrum of PSA@Fe_3O_4@SiO_2, two new peaks assigned to photoelectrons originating from the Si 2s and Si 2p energy level appear at 154 and 103 eV, respectively, and characteristic peaks of Fe $2p_{3/2}$ and Fe $2p_{1/2}$ disappear.[53] From these results, we can conclude that Fe_3O_4 decorated PSA nanoparticles were completely encapsulated by silica layer. PSA@Fe_3O_4@SiO_2-DMH nanoparticles exhibit the peaks of C 1s, O 1s, Si 2s, Si 2p, and a new N 1s peak at 400 eV, in response to the amide group of hydantoin groups.[54]

The deposition of Fe_3O_4 on PSA nanoparticles was further verified from the XRD and EDX data which were collected from the PSA@Fe_3O_4 sample. Figure 4a shows the typical XRD pattern of the obtained PSA@Fe_3O_4 nanoparticles. All the observed peaks in the pattern can be indexed to the face-centered-cubic phase of Fe_3O_4.[55] No impurity is observed, which indicates that the product is pure Fe_3O_4 phase. Moreover, a broad peak appearing in the range from 15° to 25° is attributed to amorphous PSA.[46] The EDX spectrum (Figure 4b) of PSA@Fe_3O_4 nanoparticles demonstrates the existence of O, C, and Fe element, of which the Fe element arises from Fe_3O_4. The Au peaks in the spectrum come from Au deposited on the tested sample before measurement. These XRD and EDX data suggest that the PSA nanoparticles were coated by the Fe_3O_4 nanoparticles.

The mass ratio of Fe_3O_4 to PSA has a dramatic impact on the morphology of the PSA@Fe_3O_4 nanoparticles. As shown in TEM images (Figure 5), with increasing Fe_3O_4/PSA ratio from 1/1 to 3/1, then to 5/1, the surfaces of PSA@Fe_3O_4 nanoparticles become more and more rough. When the Fe_3O_4/PSA ratio is 1/1, Fe_3O_4 is not sufficient to cover the whole PSA nanoparticles, leaving some bare PSA particles without Fe_3O_4 decoration. When the Fe_3O_4/PSA ratio is 3/1, PSA particle surfaces can be uniformly surrounded by Fe_3O_4, forming perfect Fe_3O_4-decorated magnetic PSA nanoparticles. When the Fe_3O_4/PSA ratio is 5/1, Fe_3O_4 is excessive, and some aggregated Fe_3O_4 nanoparticles without PSA core was generated while PSA nanoparticles were fully functionalized with Fe_3O_4. Therefore, in the subsequent silica coating, PSA@Fe_3O_4 nanoparticles prepared with

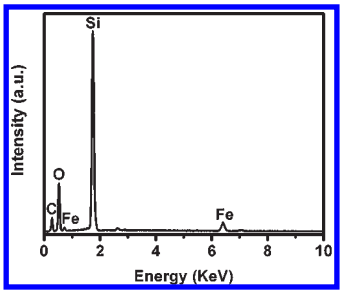

Figure 6. EDX spectrum of PSA@Fe_3O_4@SiO_2 nanoparticles.

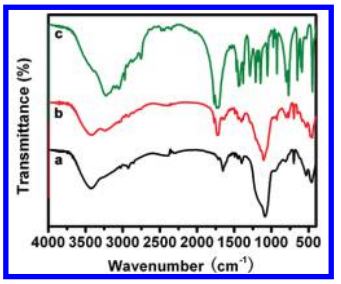

Figure 7. FTIR spectra of (a) PSA@Fe_3O_4@SiO_2, (b) PSA@Fe_3O_4@SiO_2-DMH nanoparticles, and (c) free DMH.

Fe_3O_4/PSA ratio of 3/1 were employed to fabricate PSA@Fe_3O_4@SiO_2 nanoparticles.

As a result of anisotropic dipolar attraction, magnetic Fe_3O_4 nanoparticles tend to aggregate together, and silica coating through a sol−gel process can well tackle this problem. Silica coating can effectively screen the magnetic dipolar attraction between Fe_3O_4 nanoparticles, and favor the stability of Fe_3O_4 nanoparticles immobilized on PSA surfaces. Furthermore, this coating provides them with a silica surface, possessing a larger amount of terminated silanol, which allows further modification with various groups through well-developed silane chemistry that are useful for practical applications. To coat a silica layer, TEOS as precursor of SiO_2 was first adsorbed uniformly onto PSA@Fe_3O_4 nanoparticles under the condition of continuous stirring. Because there are large amount of functional groups on the PSA@Fe_3O_4 particles surfaces, which enhance the affinity between the nanoparticles and TEOS. Silica layer was formed on the PSA@Fe_3O_4 surfaces via the hydrolysis and polycondensation of TEOS in an aqueous-ethanolic medium when ammonium hydroxide was added.[50] In the EDX spectrum (Figure 6), besides O, C, and Fe element of PSA@Fe_3O_4 nanoparticles, Si element from SiO_2 layer is observed, which is in good agreement with the TEM and XPS result (Figures 2d and 3c).

Immobilization of DMH on PSA@Fe_3O_4@SiO_2 nanoparticles was further confirmed by FTIR analyses. Figure 7 shows FTIR spectra of free DMH and of PSA@Fe_3O_4@SiO_2 nanoparticles before and after DMH immobilization. The vibrational peak at 3242 cm^{-1} assigned to the N−H bending vibration of the hydantoin group was present in the spectrum of PSA@Fe_3O_4@SiO_2-DMH nanoparticles.[56] It can also be observed that another obvious vibrational peak at 1700 cm^{-1} appeared, which was attributed to the C═O amide stretching of the hydantoin groups from DMH molecule.[56] Therefore, the FTIR technique further verified that DMH has been successfully loaded onto PSA@Fe_3O_4@SiO_2 nanoparticles.

The effect of mass ratio of DMH to PSA@Fe_3O_4@SiO_2−CPS on the DMH loading on PSA@Fe_3O_4@SiO_2 nanoparticles was

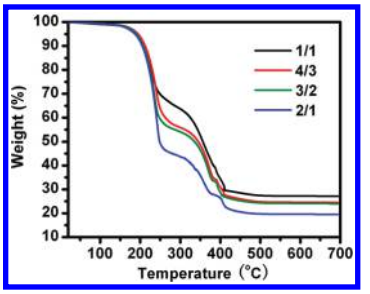

Figure 8. TGA curves of PSA@Fe_3O_4@SiO_2-DMH nanoparticles prepared with different DMH/PSA@Fe_3O_4@SiO_2−CPS mass ratio.

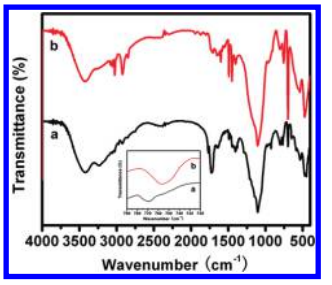

Figure 9. FTIR spectra of PSA@Fe_3O_4@SiO_2-DMH (a) and *N*-halamine-immobilized PSA@Fe_3O_4@SiO_2 (b) nanoparticles. Insert is the enlarged version of the FTIR spectra between 720 and 790 cm^{-1}.

investigated by means of varying the DMH/PSA@Fe_3O_4@SiO_2−CPS mass ratio from 1/1 to 4/3, to 3/2, then to 2/1, whereas all the other reaction parameters were kept constant. The thermogravimetric analysis (TGA) results of the as-prepared PSA@Fe_3O_4@SiO_2-DMH with different DMH loadings are illustrated in Figure 8. From TGA information, we can conclude that these samples have the same component whereas different content. The weight loss below 200 °C is attributed to the evaporation of water and residual organic solvent.[57] The nanoparticles begin decomposing at about 220 °C, which is ascribed to the decomposition of DMH.[57] The decomposition rate increases at 320 °C, which is caused by the degradation of the PSA component, and the PSA completely disappeared at about 500 °C.[58] The incombustible residues remaining after pyrolysis are assumed to be the mixture of Fe_3O_4 and SiO_2.[59] It is obvious that the content of incombustible residues decrease from 27 to 19 wt % as the increase in DMH/PSA@Fe_3O_4@SiO_2−CPS mass ratio ranged from 1/1 to 2/1. As for PSA@Fe_3O_4@SiO_2-DMH nanoparticles, the content of the incombustible residues decreases with the increased DMH loading. Therefore, we can conclude that the DMH loading on PSA@Fe_3O_4@SiO_2 nanoparticles increases as the DMH/PSA@Fe_3O_4@SiO_2−CPS mass ratio increases.

After chlorination, DMH immobilized on surface of PSA@Fe_3O_4@SiO_2 nanoparticles transforms into *N*-halamine structure, obtaining *N*-halamine-immobilized PSA@Fe_3O_4@SiO_2 nanoparticles, which can be captured by FTIR measurement. Figure 9 illustrated FTIR spectra of PSA@Fe_3O_4@SiO_2-DMH and *N*-halamine-immobilized PSA@Fe_3O_4@SiO_2. The characteristic absorption bands at 1628, 1495, and 1452 cm^{-1} for C═C stretching and 754 cm^{-1} for C−H bending of benzene ring are clearly observed.[60] The peak at 700 cm^{-1} is attributed to corrugation vibration of benzene ring, and the peaks at 1705 and 1451 cm^{-1} are the characteristic absorption bands of carboxyl

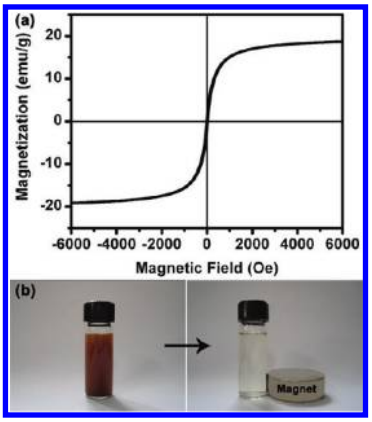

Figure 10. (a) Magnetization curve of the *N*-halamine-immobilized PSA@Fe_3O_4@SiO_2 nanoparticles at 298 K. (b) Photographs of the *N*-halamine-immobilized PSA@Fe_3O_4@SiO_2 nanoparticles dispersed in aqueous solution without and with external magnetic field.

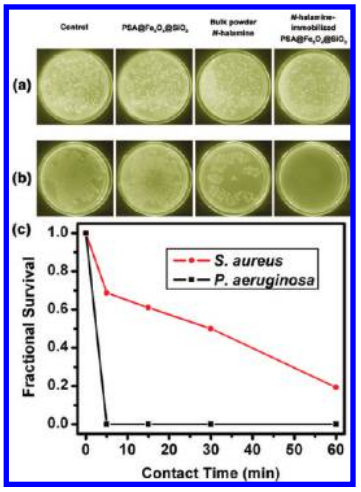

Figure 11. Photographs showing the bacterial culture plates of (a) *S. aureus* and (b) *P. aeruginosa* upon a 30 min exposure of the control, PSA@Fe_3O_4@SiO_2 nanoparticles, bulk powder *N*-halamine, and *N*-halamine-immobilized PSA@Fe_3O_4@SiO_2 nanoparticles. (c) Antibacterial kinetic test graphs for the *N*-halamine-immobilized PSA@Fe_3O_4@SiO_2 nanoparticles against *S. aureus* and *P. aeruginosa* as a function of contact time.

groups of acrylic acid.[60,61] The peak at 534 cm^{-1} is ascribed to the stretching vibration of Fe−O bands.[62] The peak at 957 cm-1 is attributed to the stretching of Si−OH, and the two peaks at 800 and 1100 cm-1 arise from the symmetric and antisymmetric stretching vibration of Si−O−Si bond, respectively.[63] These peaks mentioned above are observed in both these two curves. In the case of PSA@Fe_3O_4@SiO_2-DMH nanoparticles, the broad peaks centered at 3253 and 1750 cm^{-1} are attributed to the stretching vibration of N−H and C═O bond from DMH, respectively.[56] As for *N*-halamine-immobilized PSA@Fe_3O_4@SiO_2 nanoparticles, the broad peak corresponding to the stretching vibration of N−H bond disappears, and a new peak at 756 cm^{-1} assigned to the N−Cl group is detected.[56] An enlarged version of the FTIR spectra between 720 and 790 cm^{-1} clearly indicates presence of the N−Cl bonds.

Our group has reported that *N*-halamine-functionalized silica−polymer core−shell nanoparticles could be produced by the encapsulation of silica nanoparticles as support with polymeric *N*-halamine.[64] For further practical application, *N*-halamine-immobilized PSA@Fe_3O_4@SiO_2 nanoparticles combining magnetic property and antibacterial performance into one single entity were fabricated. This rational combination can make the *N*-halamine-based antibacterial materials magnetically separable and widen their applications. Furthermore, regenerability is a significant feature of *N*-halamine structural antibacterial, and introducing the magnetic component can make the *N*-halamine structural antibacterial materials recyclable.[20,21] The magnetic behavior of *N*-halamine-immobilized PSA@Fe_3O_4@SiO_2 nanoparticles was investigated using a superconducting quantum interference device magnetometer. The *M*-*H* curve measurements (Figure 10a) of the sample indicate that the products inherit the superparamagnetic property from the Fe_3O_4 nanoparticles, and its saturation magnetization value (M_s) is 18.93 emu·g^{-1}. This M_s is much lower than that of the corresponding bulk Fe_3O_4, which may be due to the small size of the Fe_3O_4 nanoparticles and the diamagnetic contribution of the silica shell surrounding the magnetite nanoparticles.[65] The magnetic targeting of *N*-halamine-immobilized PSA@Fe_3O_4@SiO_2 nanoparticles was tested in aqueous solution by placing a magnet near the glass bottle (Figure 10b). The nanoparticles were attracted toward the magnet within short time. Therefore, this kind of nanoparticles could carry antibacterial *N*-halamines to the targeted location of bacterial colonies, and also recover them after antibacterial behavior by the aid of an external magnetic field. These nanoparticles are potent biocidal agents, which can be easily separated and mechanically directed by applying a magnet. This is a utility when a particle-bound bacteria needs to be captured for environmental monitoring, or the particles are to be directed specifically to be a location of bacterial colonies, such as in water treatment system and cooling devices and pipes.

The antibacterial performance of the *N*-halamine-immobilized PSA@Fe_3O_4@SiO_2 nanoparticles was examined against Gram-positive bacteria *Staphylococcus aureus* (*S. aureus*) and Gram-negative bacteria *Pseudomonas aeruginosa* (*P. aeruginosa*) by using the spread plate method. For comparison, the antibacterial assay of the pure PSA@Fe_3O_4@SiO_2 nanoparticles and bulk powder *N*-halamine were carried out by the same method. Figure 11a and 11b show photographs of the bacterial culture plates, visualizing the survival case of bacteria after 30 min exposure to the control, PSA@Fe_3O_4@SiO_2, bulk powder *N*-halamine, and *N*-halamine-immobilized PSA@Fe_3O_4@SiO_2 nanoparticles. The bacteria colonies on the culture plates are observed as small white dots.[66] No significant difference was noticed between the control and PSA@Fe_3O_4@SiO_2 nanoparticles, whereas obvious decrease was detected in the population of the bacterial colonies after the exposure to the bulk powder *N*-halamine and *N*-halamine-immobilized PSA@Fe_3O_4@SiO_2 nanoparticles. Accordingly, it is considered that the PSA@Fe_3O_4@SiO_2 nanoparticles have no antibacterial function at all, and the antibacterial performance of the *N*-halamine-immobilized PSA@Fe_3O_4@SiO_2 nanoparticles is provided by the *N*-halamine structures. Compared with bulk powder *N*-halamine, the *N*-halamine-immobilized PSA@Fe_3O_4@SiO_2 nanoparticles showed excellent antibacterial activity against both *S. aureus* and *P. aeruginosa*. The improvement in the antibacterial performance can be explained by the large surface area of the *N*-halamine-immobilized PSA@Fe_3O_4@SiO_2 nanoparticles. The antibacterial agents with larger surface area can provide more active sites to contact the bacteria, and thus display the enhanced antibacterial activity.

Table 1. Minimum Inhibitory Concentration (MIC) and Minimum Bactericidal Concentration (MBC) of the *N*-Halamine-Immobilized PSA@Fe_3O_4@SiO_2 Nanoparticles against *S. aureus* and *P. aeruginosa*

bacteria	MIC (mg/mL)	MBC (mg/mL)
S. aureus	80	>160
P. aeruginosa	60	80

Table 2. Fractional Survival of Bacterial Colonies after the Exposure to *N*-Halamine-Immobilized PSA@Fe_3O_4@SiO_2 Nanoparticles for Different Contact Time

	fractional survival[a]	
contact time (min)	*S. aureus*	*P. aeruginosa*
0	1.00	1.00
5	0.69	0
15	0.61	0
30	0.50	0
60	0.19	0

[a] Fractional survival = B/A; where A is the number of surviving bacteria colonies on the control plate and B is that on the sample plate.

Minimum inhibitory concentration (MIC) and minimum bactericidal concentration (MBC) value of the *N*-halamine-immobilized PSA@Fe_3O_4@SiO_2 nanoparticles were also determined to study their quantitative antibacterial properties. The MIC was defined as the sample concentration at which the colonies were reduced in the CFU/mL numbers of ≥3 log and MBC was defined as the sample concentration at which no colony was visual.[67] As shown in Table 1, the *N*-halamine-immobilized PSA@Fe_3O_4@SiO_2 nanoparticles have the MIC value of 80 mg/mL against *S. aureus* and 60 mg/mL against *P. aeruginosa*. And the MBC value against *S. aureus* is higher than 160 mg/mL, which is higher than the MBC value of 80 mg/mL against *P. aeruginosa*. Therefore, it is considered that these nanoparticles have higher antibacterial efficacy against *P. aeruginosa* than *S. aureus*, which can be further verified by the antibacterial kinetic test. Figure 11c shows the antibacterial performance of *N*-halamine-immobilized PSA@Fe_3O_4@SiO_2 nanoparticles against *S. aureus* and *P. aeruginosa* as a function of contact time. The fractional survival of bacterial colonies after the exposure to *N*-halamine-immobilized PSA@Fe_3O_4@SiO_2 nanoparticles with different contact time is given in Table 2. As a general observation, the nanoparticles provided faster antibacterial action against *P. aeruginosa* than *S. aureus* within the contact time ranged from 0 to 60 min. For example, the nanoparticles inactivated 31% *S. aureus* after 5 min and killed 81% *S. aureus* even after 60 min, whereas in the case of *P. aeruginosa*, the nanoparticles need a contact time of less than 5 min to execute the total kill. Therefore, it is considered that *P. aeruginosa* would be more vulnerable than *S. aureus* against the *N*-halamine-immobilized PSA@Fe_3O_4@SiO_2 antibacterial agents.

For antibacterial test, the sample concentration varied from 1.25 to 2.5, to 5, to 10, to 20, to 40, to 60, to 80, to 100, to 160, to 200, then to 300 mg/mL, and 200 mg/mL was found to be the most suitable. Lower concentration leaded to unconspicuous antibacterial activity, and higher concentration was unnecessary. Compared with those concentrations with the range from 0 to 1000 μg/mL reported in the previous papers, these concentrations seem to be quite high.[14,15] However, the *N*-halamine content of the as-synthesized product is low, and thus the effective *N*-halamine concentration of the product is far lower than 200 mg/mL. For another, to the best of our knowledge, versatile antibacterial organic materials, including quaternary ammonium salt, phosphonium salt, halogenated sulphonamide group, *N*-halamine, and guanidine have been widely investigated, and the mode of biocidal action of these antibacterial agents is quite different.[18] Therefore, it is difficult to determine which kind of biocide has advantage over the others only depending on the sample concentration. Besides sample concentration, antibacterial difference between two kinds of antibacterial agents is attributed to many parameters such as particle size, contact time, surface area, microorganism type, and biocidal mechanism.[19]

CONCLUSION

We have presented an efficient method for the design and preparation of magnetic/antimicrobial bifunctional nanoparticles through immobilization of antibacterial *N*-halamine on silica-coated magnetic PSA nanoparticles. The *N*-halamine was developed from the precursor DMH by chlorination treatment, and the loading amount of DMH on the silica-coated Fe_3O_4-decorated poly(styrene-*co*-acrylate acid) nanoparticles was controllable. The *N*-halamine-immobilized PSA@Fe_3O_4@SiO_2 nanoparticles show superparamagnetic behavior, as well as powerful antibacterial property, with disinfection capability within a few minutes of contact time. Due to the larger surface area, the resultant nanoparticles displayed higher antibacterial activity against both *P. aeruginosa* and *S. aureus* than their bulk counterparts. Therefore, these bifunctional nanoparticles synthesized in this study possess considerable potential for use in medical devices, healthcare products, water purification systems, hospitals, dental office equipment, food packaging, food storage, household sanitation, etc.

AUTHOR INFORMATION

Corresponding Author

*Tel: +86-431-82276325. Fax: +86-431-88499187. E-mail: gaoge@jlu.edu.cn (G.G.); chen_yuxin@jlu.edu.cn (Y.C.).

ACKNOWLEDGMENT

We thank the National Natural Science Foundation of China (50673033) and the National Natural Science Foundation of Jilin Province (201115011) for financial support.

REFERENCES

(1) Barnes, K.; Liang, J.; Wu, R.; Worley, S. D.; Lee, J.; Broughton, R. M.; Huang, T. S. *Biomaterials* **2006**, *27*, 4825–4830.
(2) Urbansky, E. T. *Chem. Rev.* **2001**, *101*, 3233–3243.
(3) Richardson, S. D. *Anal. Chem.* **2007**, *79*, 4295–4324.
(4) Debiemme-Chouvy, C.; Haskouri, S.; Folcher, G.; Cachet, H. *Langmuir* **2007**, *23*, 3873–3879.
(5) Biswas, K.; Craik, S.; Smith, D. W.; Belosevic, M. *Water Res.* **2003**, *37*, 4737–4747.
(6) Flyunt, R.; Leitzke, A.; Mark, G.; Mvula, E.; Reisz, E.; Schick, R.; von Sonntag, C. *J. Phys. Chem. B* **2003**, *107*, 7242–7253.
(7) Sinkaset, N.; Nishimura, A. M.; Pihl, J. A.; Trogler, W. C. *J. Phys. Chem. A* **1999**, *103*, 10461–10469.

(8) Li, Y.; Leung, W. K.; Yeung, K. L.; Lau, P. S.; Kwan, J. K. C. *Langmuir* **2009**, *25*, 13472–13480.
(9) Ran, X.; Wang, L.; Cao, D.; Lin, Y.; Hao, J. *Appl. Organomet. Chem.* **2011**, *25*, 9–15.
(10) Waschinski, C. J.; Zimmermann, J.; Salz, U.; Hutzler, R.; Sadowski, G.; Tiller, J. C. *Adv. Mater.* **2008**, *20*, 104–108.
(11) Song, J.; Kong, H.; Jang, J. *Colloids Surf. B: Biointerfaces* **2011**, *82*, 651–656.
(12) Kenawy, E.; Abdel-Hay, F. I.; El-Shanshoury, A. E. R.; El-Newehy, M. H. *J. Polym. Sci., Part A: Polym. Chem.* **2002**, *40*, 2384–2393.
(13) Shen, X.; Ye, G.; Cheng, X.; Yu, C.; Yao, H.; Hu, C. *J. Pept. Sci.* **2010**, *16*, 58–64.
(14) Bromberg, L.; Chang, E. P.; Alvarez-Lorenzo, C.; Magariños, B.; Concheiro, A.; Hatton, T. A. *Langmuir* **2010**, *26*, 8829–8835.
(15) Bromberg, L.; Chang, E. P.; Hatton, T. A.; Concheiro, A.; Magariños, B.; Alvarez-Lorenzo, C. *Langmuir* **2011**, *27*, 420–429.
(16) Emerson, D. W. *Ind. Eng. Chem. Res.* **1990**, *29*, 448–450.
(17) Ahmed, A. E. I.; Hay, J. N.; Bushell, M. E.; Wardell, J. N.; Cavalli, G. *React. Funct. Polym.* **2008**, *68*, 1448–1458.
(18) Jang, J.; Kim, Y. *Chem. Commun.* **2008**, 4016–4018.
(19) Kenawy, E.; Worley, S. D.; Broughton, R. *Biomacromolecules* **2007**, *8*, 1359–1384.
(20) Kocer, H. B.; Akdag, A.; Worley, S. D.; Acevedo, O.; Broughton, R. M.; Wu, Y. *ACS Appl. Mater. Interfaces* **2010**, *2*, 2456–2464.
(21) Sun, Y.; Sun, G. *Macromolecules* **2002**, *35*, 8909–8912.
(22) Ren, X.; Kou, L.; Liang, J.; Worley, S. D.; Tzou, Y.; Huang, T. S. *Cellulose* **2008**, *15*, 593–598.
(23) Barnes, K.; Liang, J.; Worley, S. D.; Lee, J.; Broughton, R. M.; Huang, T. S. *J. Appl. Polym. Sci.* **2007**, *105*, 2306–2313.
(24) Akdag, A.; Kocer, H. B.; Worley, S. D.; Broughton, R. M.; Webb, T. R.; Bray, T. H. *J. Phys. Chem. B* **2007**, *111*, 5581–5586.
(25) Liang, J.; Wu, R.; Wang, J. W.; Barnes, K.; Worley, S. D.; Cho, U.; Lee, J.; Broughton, R. M.; Huang, T. S. *J. Ind. Microbiol. Biotechnol.* **2007**, *34*, 154–163.
(26) Makal, U.; Wood, L.; Ohman, D. E.; Wynne, K. I. *Biomaterials* **2006**, *27*, 1316–1326.
(27) Coulliette, A. D.; Peterson, L. A.; Mosberg, J. A.; Rose, J. A. *Am. J. Trop. Med. Hyg.* **2010**, *82*, 279–288.
(28) Sun, Y.; Sun, G. *Ind. Eng. Chem. Res.* **2004**, *43*, 5015–5020.
(29) Chen, M.; Xie, L.; Li, F.; Zhou, S.; Wu, L. *ACS Appl. Mater. Interfaces* **2010**, *2*, 2733–2737.
(30) Mohammed, J. S.; McShane, M. *Langmuir* **2008**, *24*, 13796–13803.
(31) Costi, R.; Saunders, A. E.; Banin, U. *Angew. Chem., Int. Ed.* **2010**, *49*, 4878–4897.
(32) Lek, J. Y.; Xi, L.; Kardynal, B. E.; Wong, L. H.; Lam, Y. M. *ACS Appl. Mater. Interfaces* **2011**, *3*, 287–292.
(33) Xiao, S.; Wu, S.; Shen, M.; Guo, R.; Huang, Q.; Wang, S.; Shi, X. *ACS Appl. Mater. Interfaces* **2009**, *1*, 2848–2855.
(34) Zeng, H.; Sun, S. *Adv. Funct. Mater.* **2008**, *18*, 391–400.
(35) Nykypanchuk, D.; Maye, M. M.; Lelie, D. V. D.; Gang, O. *Nature* **2008**, *451*, 549–552.
(36) Fang, J.; Wang, H.; Xue, Y.; Wang, X.; Lin, T. *ACS Appl. Mater. Interfaces* **2010**, *2*, 1449–1455.
(37) Zhao, G.; Wang, J.; Li, Y.; Chen, X.; Liu, Y. *J. Phys. Chem. C* **2011**, *115*, 6350–6359.
(38) Lee, M.; Thomas, J. L.; Ho, M.; Yuan, C.; Lin, H. *ACS Appl. Mater. Interfaces* **2010**, *2*, 1729–1736.
(39) Jun, B.; Kim, G.; Baek, J.; Kang, H.; Kim, T.; Hyeon, T.; Jeong, D. H.; Lee, Y. *Phys. Chem. Chem. Phys.* **2011**, *13*, 7298–7303.
(40) Fakhrullin, R. F.; Bikmullin, A. G.; Nurgaliev, D. K. *ACS Appl. Mater. Interfaces* **2009**, *1*, 1847–1851.
(41) Massart, R. *IEEE Trans. Magn.* **1981**, *17*, 1247–1248.
(42) Jayawardena, K. D. G. I.; Fryar, J.; Silva, S. R. P.; Henley, S. J. *J. Phys. Chem. C* **2010**, *114*, 12931–12937.
(43) Dong, Q.; Wang, Y.; Peng, L.; Zhang, H.; Liu, B. *Nanotechnology* **2011**, *22*, 215604.
(44) Meng, Z.; Xue, C.; Lu, L.; Yuan, B.; Yu, X.; Xi, K.; Jia, X. *J. Colloid Interface Sci.* **2011**, *356*, 429–433.
(45) Li, J.; Ma, W.; Wei, C.; Guo, J.; Hu, J.; Wang, C. *J. Mater. Chem.* **2011**, *21*, 5992–5998.
(46) Xuan, S.; Jiang, W.; Gong, X.; Hu, Y.; Chen, Z. *J. Phys. Chem. C* **2009**, *113*, 553–558.
(47) Fu, X.; Lin, L.; Wang, D.; Hu, Z.; Song, C. *Colloids Surf., A* **2005**, *262*, 216–219.
(48) Lu, Z.; Qin, Y.; Fang, J.; Sun, J.; Li, J.; Liu, F.; Yang, W. *Nanotechnology* **2008**, *19*, 055602.
(49) Ma, Z. Y.; Dosev, D.; Nichkova, M.; Gee, S. J.; Hammock, B. D.; Kennedy, I. M. *J. Mater. Chem.* **2009**, *19*, 4695–4700.
(50) Stöber, W.; Fink, A.; Bohn, E. *J. Colloid Interface Sci.* **1968**, *26*, 62–69.
(51) Xu, Z.; Li, C.; Kang, X.; Yang, D.; Yang, P.; Hou, Z.; Lin, J. *J. Phys. Chem. C* **2010**, *114*, 16343–16350.
(52) Tian, Y.; Yu, B.; Li, X.; Li, K. *J. Mater. Chem.* **2011**, *21*, 2476–2481.
(53) Deng, Z.; Chen, M.; Wu, L. *J. Phys. Chem. C* **2007**, *111*, 11692–11698.
(54) Xuan, S.; Wang, Y. J.; Leung, K. C.; Shu, K. *J. Phys. Chem. C* **2008**, *112*, 18804–18809.
(55) Teng, Z.; Li, J.; Yan, F.; Zhao, R.; Yang, W. *J. Mater. Chem.* **2009**, *19*, 1811–1815.
(56) Sun, Y.; Sun, G. *J. Appl. Polym. Sci.* **2001**, *80*, 2460–2467.
(57) Dong, A.; Zhang, Q.; Wang, T.; Wang, W.; Liu, F.; Gao, G. *J. Phys. Chem. C* **2010**, *114*, 17298–17303.
(58) Yao, T.; Lin, Q.; Zhang, K.; Zhao, D.; Lv, H.; Zhang, J.; Yang, B. *J. Colloid Interface Sci.* **2007**, *315*, 434–438.
(59) Zhao, L.; Gao, C.; Xu, W. *Langmuir* **2010**, *26*, 11217–11225.
(60) Gao, B.; Qi, C.; Liu, Q. *Appl. Surf. Sci.* **2008**, *254*, 4159–4165.
(61) Sun, Y.; Wang, B.; Wang, H.; Jiang, J. *J. Colloid Interface Sci.* **2007**, *308*, 332–336.
(62) Sun, P.; Zhang, H.; Liu, C.; Fang, J.; Wang, M.; Chen, J.; Zhang, J.; Mao, C.; Xu, S. *Langmuir* **2010**, *26*, 1278–1284.
(63) Xu, P.; Wang, H.; Tong, R.; Du, Q.; Zhong, W. *Colloid Polym. Sci.* **2006**, *284*, 755–762.
(64) Dong, A.; Huang, J.; Lan, S.; Wang, T.; Xiao, L.; Wang, W.; Zhao, T.; Zheng, X.; Liu, F.; Gao, G.; Chen, Y. *Nanotechnology* **2011**, *22*, 295602.
(65) Guo, J.; Yang, W.; He, J.; Chen, J. *Chem. Mater.* **2006**, *18*, 5554–5562.
(66) Song, J.; Kong, H.; Jang, J. *Chem. Commun.* **2009**, 5418–5420.
(67) Qi, L.; Xu, Z.; Jiang, X.; Hu, C.; Zou, X. *Carbohyd. Res.* **2004**, *339*, 2693–2700.